· Article ·
doi: 10.13679/j.advps.2016.4.00245

Advances in Polar Science
December 2016 Vol. 27 No. 4: 245-263

Outflow from under the Pine Island Bay Ice Shelf: finescale structure and its temporal variability

Robin Robertson[1,2*]

[1] School of Physical, Environmental, and Mathematical Sciences, University of New South Wales, Canberra ACT 2610, Australia;

[2] Department of Marine Science, Nanjing University of Information Science and Technology, Nanjing 210044, China

Received 31 October 2016; accepted 25 December 2016

Abstract The water column structure of the ice shelf cavity outflow from under Pine Island Glacier and its temporal variability were investigated using a hourly time series of yo-yo CTD and LADCP data collected over ~24 h at the southern end of the ice shelf front. The primary water types present over the continental shelf off Pine Island Bay were Circumpolar Deep Water (CDW), modified Circumpolar Deep Water (mCDW), Shelf Water (SW), and Ice Shelf Water (ISW). As CDW transited the shelf, it transitioned into cooler, mCDW. In the upper 200 m, ISW dominated within 100 km of the ice shelf and SW further offshore. Within Pine Island Bay, the water column was partitioned into two primary layers based on their behavior: an upper outflowing layer from 100 m to 450 m composed of ISW with a significant meltwater component, 1%–2%, over an inflowing layer from ~550 m to the sea bed composed of mCDW. Due to the small cavity extent, the outflowing water was warmer than the seawater freezing point. The upper ISW layer was further split into upper ISW layer #1 (100–300 m) and upper ISW layer #2 (320–450 m) with the transition coinciding with the ice shelf draft. Small step-like features with heights from 1–50 m existed within both the ISW layers and were more prominent in upper ISW layer #1. A baroclinic signal at the semidiurnal frequency existed within both primary layers with the strongest signal, ~ 10 cm·s^{-1}, propagating vertically in the upper ISW layer.

Keywords **Pine Island Bay, double-diffusion, Amundsen Sea, internal tides**

Citation: Robertson R. Outflow from under the Pine Island Bay Ice Shelf: finescale structure and its temporal variability. Adv Polar Sci, 2016, 27: 245-263, doi:10.13679/j.advps.2016.4.00245

1 Introduction

Satellite observations indicate that the Pine Island Bay Ice Shelf (PIBIS) is melting faster than other Antarctic ice shelves[1] with the ocean driving the melting[2-6] (Figure 1). "Warm" modified Circumpolar Deep Water (mCDW) enters the ice shelf cavity, fueling the melting[5-10]. Melting occurs both along the front edge of the ice shelf and at the base of ice shelf within the ice shelf cavity, particularly at the back of the cavity along the grounding line. Most of the melted ice shelf water exits at the southeastern edge of the ice shelf [8-9]. The distribution of this melted ice shelf water reaches kilometers from the ice shelf[10-11].

The recent rapid melting of PIBIS has been attributed in part to both climatic changes[5,11] and changes in the topography of the ice cavity[6,8,10] . The topographic change occurred with the breaching of a ridge within the PIBIS cavity, moving the grounding line, and opening up a new chamber within the cavity where the additional basal melting occurs[6,8]. The ice shelf melting is influenced both by the circulation within the ice shelf cavity and by the water mass(es) flowing into it. Changes in climatic conditions are increasing the volume and temperature of the available warm water for melting[5,11].

The basic circulation is "warm", salty, mCDW enters the cavity in the bottom portion of the water column. When it comes in contact with the ice shelf, the "warm" water melts the ice, becoming cooler and fresher as the new melt water joins the former mCDW. This mix is denoted Ice Shelf Water (ISW) and is fresher, cooler, and less dense than the mCDW. The ISW cycle for the PIBIS cavity is primarily driven by the horizontal density gradients that develop between the ice shelf

* Corresponding author, E-mail: r.robertson@adfa.edu.au

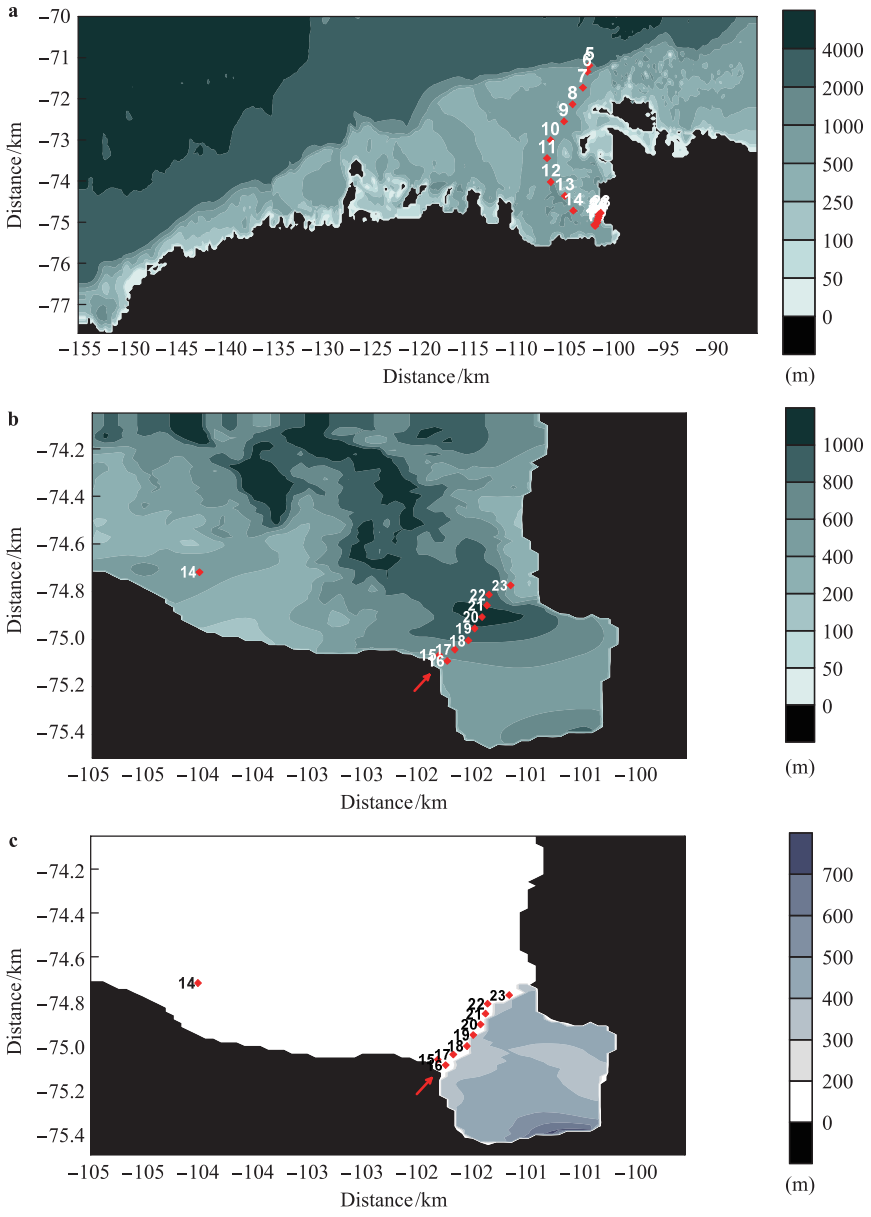

Figure 1 Bathymetry for the Amundsen Sea taken from Timmermann et al.[12] (**a**) and ice shelf thickness for Pine Island Bay (PIB) in the Amundsen Sea (**b**, **c**). The topography in (**b**) and (**c**) were adjusted according to data taken from Nitsche et al.[13-14] so the ship locations would not be aground. CTD/LADCP locations are indicated by (red) diamonds and labeled with the CTD number. The notch in the ice shelf where the yo-yo CTD/LADCP data was collected is indicated by a red arrow in (**b**) and (**c**). The Nitsche et al.[13-14] bathymetry has been updated since 2007 with the data from several cruises and is available at https://www.ldeo.columbia.edu/~fnitsche/research/AntarcticBathymetry/AntarcticBathymetry.html.

cavity and the bay due to the melting ice shelf[6,8]. However, currents, winds, and tides have been found to impact the flow and ice shelf melting[15]. Currents, such as coastal currents, push warm mCDW under the ice shelf, increasing ice shelf melting and ISW outflow. In a modeling study, tides were found to affect the circulation into and under the ice shelf, increasing inflow and the outflow to the ice shelf cavity and melting of the ice shelf by 3.3 $m \cdot a^{-1}$ (~20%), when a wind-driven gyre was present[15].

Through impacts on the flow into and within the ice shelf cavity and water mass transformation, other processes such as double diffusion, intrusions, inertial oscillations, internal waves, mixing, and changes in the water masses on the continental shelf may also play a role in ice shelf melting. Double diffusion from vertical ice walls, such as that along the ice shelf front[16-17], can form steps. Such steps were found in front of the Erebus Glacier Tongue in McMurdo Sound, Ross Sea[16]. Similarly, double diffusive steps from cool, fresh water overlaying warm, salty layer can also drive double diffusive mixing (i.e)[18]. Conditions in front of the PIBIS may be conducive for double diffusive step types to exist.

The primary mixing mechanisms for water mass transformation are wind, ISW outflow, internal tides/waves,

and double diffusion. Wind plays a role near the surface in PIB, but not within the ice shelf cavity. The ISW, which exits PIBIS cavity, is fresher and less dense than the surface water in PIB. Consequently, it rises to the surface when it exits the cavity, in a similar manner to the flow over a sill, except upside down. Large boils of water coming to the surface were observed in front of PIBIS during NBP0901(voyage 1 in 2009 on the RVIB *Nathanial B Palmer*)[13]. This mixing influences the surface water in front of the ice shelf, but not within the cavity. The primary candidate for mixing within the cavity is internal tides or waves, which often induce mixing through shear instabilities[19]. Internal tides result from the interaction of the barotropic tide with topographic features, such as the ridge in the PIBIS cavity or the front of the ice shelf. Thurnherr et al.[9] note that the variability of the observed velocities at the outflow of the ice shelf is "consistent with internal gravity waves"; however, they do not illuminate this observation, identify the frequencies of the internal waves, or otherwise quantify the statement.

Tides in PIBIS are small in elevation with weak currents, according to tidal estimates from both a regional baroclinic tidal model of PIB and its ice shelf cavity[15] and a global barotropic tidal model assimilating Topex/Poseidon, TPXO8.0[20]. From these estimates, tidal elevation amplitudes in PIB (not shown) are small, <10 cm, for the M_2 semidiurnal constituent, but are significant for the S_2 semidiurnal constituent, 18–19 cm, and the diurnal constituents, K_1, 41–42 cm, and O_1, 27–28 cm. Both models (Robertson[15] and TPX08.0) indicate small velocities, <1 cm·s^{-1}, along the ice shelf front for all four major constituents, M_2, S_2, K_1, and O_1 with the diurnal tides stronger than the semidiurnal tides.

Although the semidiurnal tides are weaker than the diurnal tides, they play a bigger role in mixing since their baroclinic response is stronger and it propagates at this latitude. PIB is far south of the diurnal critical latitudes (where the tidal frequency equals the inertial frequency) so diurnal internal tides are trapped and the response is primarily barotropic[15]. The M_2 critical latitude is at 74°28'S, which passes through PIB north of the PIBIS cavity. Consequently, M_2 baroclinic tides should only propagate in PIB north of 74°28'S and only S_2 baroclinic or internal tides can propagate in the outflow region of PIBIS cavity. However, vorticity from a wind-driven gyre present during the observations effectively shifted the critical latitude 1° poleward, enabling M_2 internal tides to propagate and a more baroclinic M_2 response[15]. It should be noted that near the critical latitude inertial oscillations are indistinguishable from semidiurnal tides without exceedingly long time series, multiple years or decades.

The hydrography and circulation of the eastern Amundsen Sea (Figure 1a) were investigated during NBP0901, focusing on the regions in front of the Pine Island, Thwaites, and Dotson ice shelves, in order to illuminate the effects of the ocean forcing on the ice shelves of the Amundsen Sea. This study examines a small portion of the data collected, specifically a time series of observational data collected at the southern portion of PIBIS where the strongest outflow was observed (arrow in Figure 1b). Note that in Figure 1b and 1c, the latitude of the bathymetry has been shifted according to the measurements of Frank Nitsche[13-14], in order that the ship and all observations were not on the continent and they followed the ice shelf front as occurred during voyage NPB0901[13]. Conductivity, Temperature, and Depth (CTD) and Lowered Acoustic Doppler Current Profiler (LADCP) data were analyzed to determine the structure of the water column and currents and their temporal variability. The goals were to: (1) characterize the outflow of PIBIS in the southern notch in the ice shelf, (2) determine the role of double diffusion, intrusions, tides, internal tides, internal waves, inertial oscillations and other mechanisms in this outflow, illuminating the predominant processes occurring in the ice shelf cavity, and (3) to determine the frequencies of the temporal fluctuations and what portion is attributable to tides. Since it is extremely difficult to make observations under the ice shelf, the best place to illuminate what is happening under the ice shelf is the outflow region. Investigating these processes within the ice shelf cavity is like looking through a key hole into a darkened room, although Jenkins et al.'s[6] autosub observations shed some light on the spatial variability of the cavity. Presently, there is no other time series at the outflow, particularly in the upper 400 m.

The observational data is composed primarily of hydrographic data from CTD casts combined with simultaneous LADCP profiles and is described in section 2. Relevant hydrography and circulation information for PIB is outlined in section 3. During NBP0901, the CTD/LADCP was operated in a yo-yo fashion in order to investigate temporal variability of the outflow. Using this yo-yo data, the structure and characteristics of the outflowing water column at the southern notch of PIBIS are described in section 4, focusing on the layers below the surface mixed layer. In section 5, the variability of the velocities that "is consistent with internal gravity waves" as noted by Thurnherr et al.[9] is quantified by examining the temporal variability of both the velocity and temperature data, including identification of the frequency distribution of the fluctuations, particularly those exceeding 2 cpd. Section 6 discusses the implications of the observations at the outflow site through their keyhole view. Finally, a summary is given in section 7.

2 CTD and LADCP data

CTD data was collected at a sampling frequency of 24 Hz with a Sea-Bird SBE 9/11 using dual sensors for potential temperature, θ, salinity, S, and dissolved oxygen, DO. The CTD was lowered at 20 m·min^{-1} from the surface to 50 m, 30 m·min^{-1} from 50 m to 100 m, and 50 m·min^{-1} below 100 m. It was raised at 50–60 m·min^{-1}. A 300 kHz RDI LADCP was attached on the CTD rosette frame looking downward, measuring horizontal velocities. CTD data was processed and averaged to provide estimates of θ, S, DO at 1 m intervals from the surface to a depth 10 m above the sea bed for CTD casts along of the PIBIS front and

the first 5 casts of the yo-yo. Eight CTD casts were made along the front of the PIBIS roughly 0.46 km from the ice shelf front, casts 16–23 on Jan 17–18, 2009 (crosses in Figure 1a). Twenty-four casts, casts 58–81, were made at one hour intervals in the southern notch of the Pine Island Glacier (PIG) at the site of cast 16 (arrow in Figure 1a) with the first one starting its descent at 21:00 GMT Jan 24, 2009 and the last one at 20:00 Jan 25, 2009. The first five casts extended to within 10 m of the sea bed and the remainder to 800 m. All casts, except the fourth, started their descents on the hour. The fourth cast was 15 min late starting its descent. A few additional CTD casts from NBP0901 are utilized, specifically an additional cast, 93, made at the location of cast 16, at 18:48 on Jan 28, 2009. Uncertainties in the potential temperature and salinity data were ± 0.002°C for θ and ± 0.002 psu for S. The LADCP data was processed using Global Positioning System (GPS) data and the Shipboard ADCP (SADCP) data to constrain the solution when combining the scans of the profile. The uncertainty in the horizontal velocities was ~1.3 cm·s^{-1}[9]. Velocity profiles of the East-West, U, and North-South, V, velocities were generated with 20 m depth bins. The velocities were then rotated by 31° to be aligned with the edge of the ice shelf front. Although the velocities were rotated to be aligned along and across the ice shelf front, the location of the yo-yo station in a notch, surrounded on three sides by ice shelf, near the southern boundary of the cavity, and with a large iceberg just offshore of its location is likely to experience steering of the currents by topographic features. Thus the along ice shelf velocity may still have a component of across ice shelf velocity in it, that cannot be compensated for or removed.

3 Hydrography and circulation in southern PIB

Although here we focus on the southern notch in the front of the PIBIS, the notch does not exist in isolation. The hydrography and circulation across the continental shelf of the Amundsen Sea and in the southern portion of PIB and the ice shelf cavity influence processes at the southern notch. Only a preliminary discussion of the data is given here, focusing on the CTD/LADCP time series. The data is discussed more fully by Jacobs et al.[8,21].

3.1 Amundsen Sea Continental Slope

Along the continental slope of the Amundsen Sea, "warm" mCDW with θ exceeding 1.0°C underlaid the cold surface mixed layer, shelf water, and winter water (0–20 km in Figure 2). The CDW flowed onto the continental shelf, primarily deeper than ~300 m, mixing and cooling as it approached PIB (>530 km in Figure 2). Nearer to PIBIS (>530 km in Figure 2), the water column was less stratified with a maximum θ difference of ~1.7°C between the surface and deep, which was roughly half of the θ difference in the water column over the continental slope. Adjacent to the ice shelf, the upper water column was warmer, fresher, and lower in dissolved oxygen (Figure 2, salinity and oxygen not shown) than it is over the continental slope. It was composed

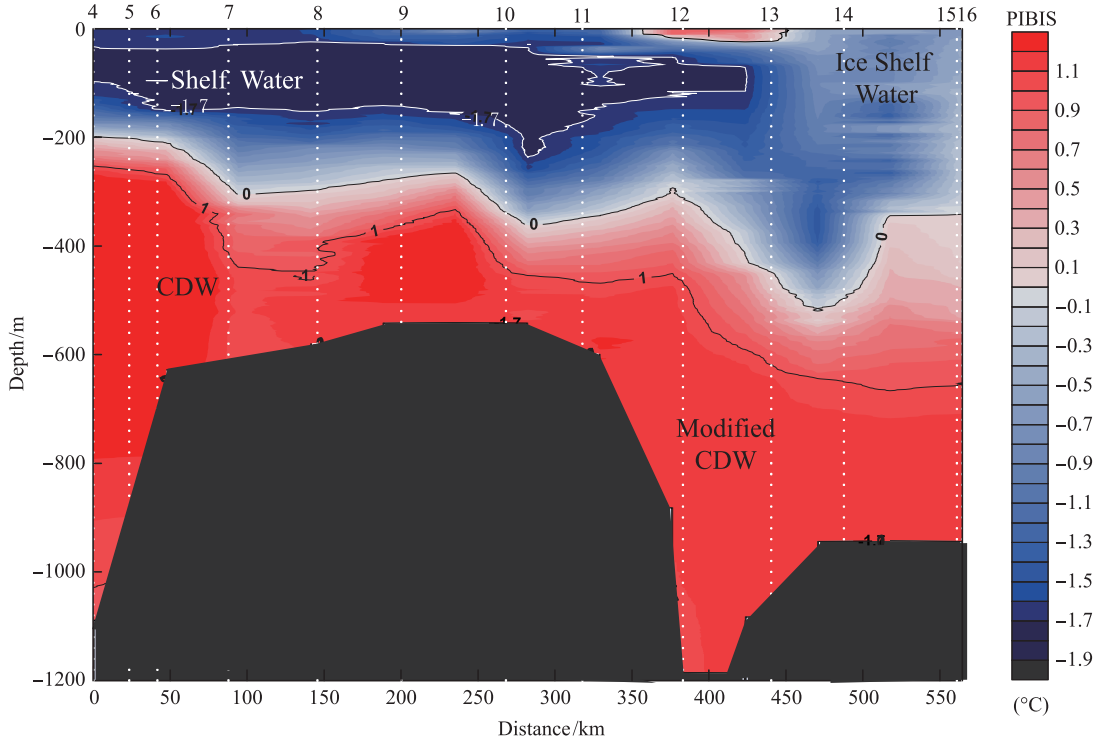

Figure 2 A transect of potential temperature from CTDs 4-16 are shown. The CTD locations are indicated by dotted vertical lines with the cast number at the top (locations given in Figure 1a. PIBIS is located at the right edge of the figure. Both the PIBIS location and the different water masses have been labeled.

of ISW with a significant meltwater component, 1%–2%, exiting the glacier[8,21]. The water column at the Northwestern and Southeastern ends of Figure 2 roughly represented the end members for the water mass mixing over the continental slope, with the offshore water column composed of shelf water over CDW and the water column in front of the ice shelf showing ISW exiting the ice shelf cavity over a cooler, mCDW (Figure 2). The two types of water interleaved with each other and evidence of these intrusions are visible between 50 and 500 m in Figure 2 (>500 km).

3.2 Flow in and out of the PIBIS cavity and in PIB

Generally, mCDW flowed into the ice shelf cavity at depth and ISW flowed out near the surface with the primary driving force for the flow being the density changes, resulting from melting of the ice shelf by the warm mCDW. In the polar regions, density is primarily controlled by salinity. To define the outflow from under the ice, a series of CTD/LADCP's were collected along the front of the ice shelf (Figure 1c). Along the ice shelf front, the water column below 550 m

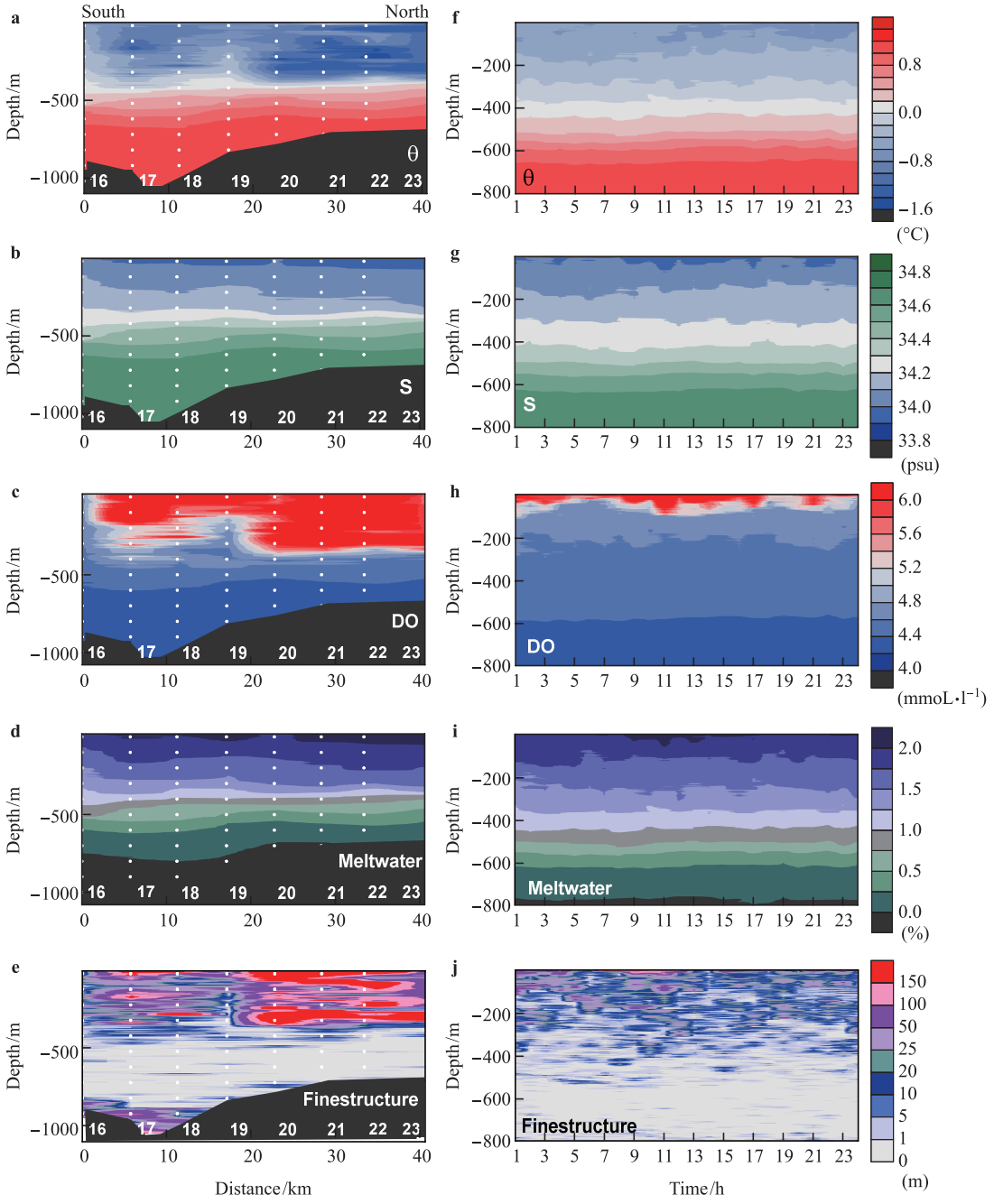

Figure 3 Transects of potential temperature (**a**), salinity (**b**), dissolved oxygen (**c**), meltwater percentage (**d**), and finestructure/Thorpe displacement (**e**) in front of the ice shelf with the southern side on the left and northern on the right. Transects of potential temperature (**f**), salinity (**g**), dissolved oxygen (**h**), meltwater percentage (**i**), and finestructure (**j**) during the 24 h CTD/LADCP yo-yo. CTD numbers are labeled at the bottom in white in the left panels.

was relatively uniform (Figures 3a and 3b). Above 550 m, the water column varied and was colder on the northern end (site of cast 23 in Figure 3) than on the southern side (site of cast 16). At the southern end of this transect (site 16 in Figure 3), the upper water was warmer (Figure 3a), saltier (Figure 3b), and lower in dissolved oxygen (Figure 3c) than at the northern end. The thermocline was deeper (Figure 3a) and meltwater percentage, as calculated following Jenkins and Jacobs[22], higher (Figure 3d) at the southern end where the yo-yo CTD data was collected.

Along the front of the ice shelf, flow into the ice shelf cavity occurred roughly below 500 m between CTD sites 17 and 21, with the strongest inflow over the trench (positive values in Figure 4a). There was also apparent inflow in the upper water column between CTD sites 18 and 22 (Figure 4a). The velocities at the southern end differed from the rest of the ice shelf front with water flowing out at all depths and the strongest flow in the upper 100 m, >35 cm·s^{-1} (Figure 4a). In the along ice shelf front direction, flow was generally southward, particularly above 200 m (Figure 4b); however, there were small patches of northward flow at CTD sites 16 and 17 deep in the water column and a strong northward flow through much of the water column at sites 21–23. This general southward flow in the upper 250 m corresponded to a gyre-like flow visible in the LADCP data when all LADCP profiles in PIB are compiled (Figure 5). The flow rotated clockwise and was centered at ~102°42'W, 74° 54'S with a maximum velocity of ~5–8 cm·s^{-1} in the upper 500 m (Figure 5). An iceberg in the northeast region of PIB prevented complete definition of the gyre (Figure 5). This

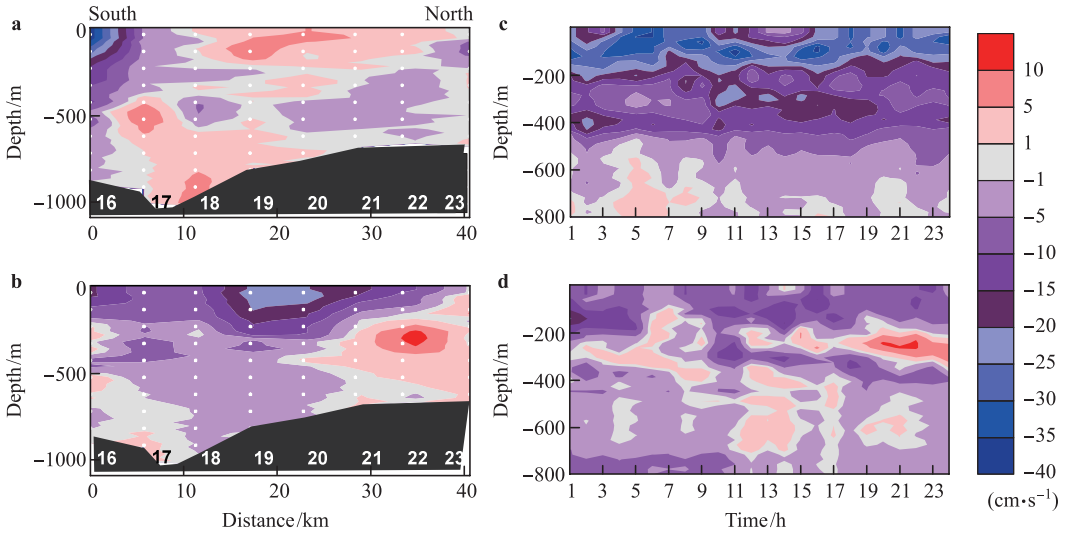

Figure 4 Mean currents across (primarily East-West) (**a**) and along (primarily North-South) ice shelf front (**b**). Positive values indicate inflow to the cavity and negative values outflow. Mean across (**c**) and along (**d**) ice shelf front currents during the yo-yo, respectively. CTD numbers are labeled at the bottom in white in (**a**) and (**b**).

is well outlined in Thurnherr et al.[9]. The along ice shelf front velocity in the upper 300 m agreed with this gyre circulation. Additionally, at the southern end near CTD site 16, a large iceberg was grounded and steered the flow around it, pushing the flow further south.

4 Water column structure

In the southern notch of PIBIS, the mean θ and S gradually increased with depth from 50 m to 800 m with noticeable changes in slope at ~500 and 600 m. (blue and green lines in Figure 6a, respectively). A more detailed look at all the profiles from the yo-yo (Figure 7) showed most of the increases above 550 m occurred at discrete depths in a series of step-like features, with "step" heights ranging from 20–120 m, although smaller "steps" down to the data averaging band of 1 m were also present. Generally, larger "steps", ~100 m height, appeared higher in the water column, whereas below 300 m, "steps" tended to be 50 m or less in height. Interspersed at irregular intervals on the large "steps"

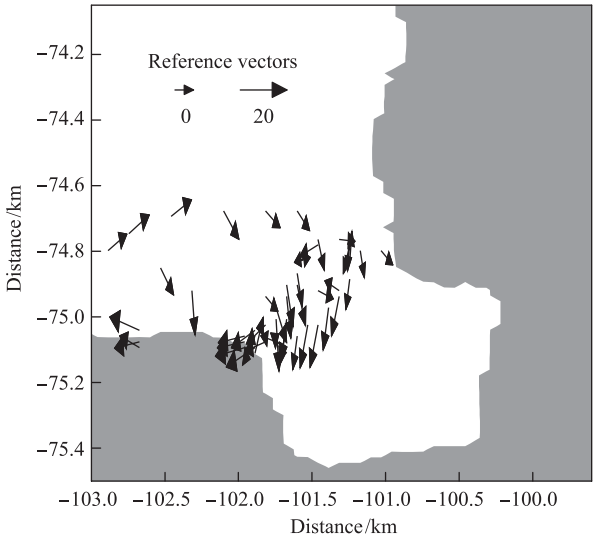

Figure 5 The presence of a gyre in PIB as determined by the LADCP velocities in the upper 500 m.

were sections with small "steps" forming gradient regions, usually not more than 50 m in height. Between 50 and 350 m, intrusions were superimposed on the step-like structure of the water column (Figure 7). The lower water column, below 600 m, showed a very gradual increase in θ (Figures 6 and 7), with some steppy structure, but no evidence of intrusions.

The mean velocities were also depth-dependent with both U (red line in Figure 6b) and V (blue line in Figure 6b) generally decreasing in magnitude with depth below their peaks of 28 cm·s^{-1} and 8 cm·s^{-1} at ~120 m and 140 m, respectively. Values at 550 m were 2.5 cm·s^{-1} and ~0.2 cm·s^{-1} for U and V, respectively. Velocities below 550 m were small, < 4 cm·s^{-1}. Rotation of the velocities by 31° (off the East-West horizontal) to align with the exit passage for the outflow from the notch did not significantly change these results. No other rotation was applied to the data. U indicates the flow out of the notch and V the flow across the notch. Substantial structure was seen in the mean velocities, with U having two distinct peaks of ~28 cm·s^{-1} and 14 cm·s^{-1} at ~120 and 400 m and V two peaks of ~8 cm·s^{-1} and 4 cm·s^{-1}, at ~140 and 300–420 m, respectively. The mean velocities indicated a northwestward flow out of the notch.

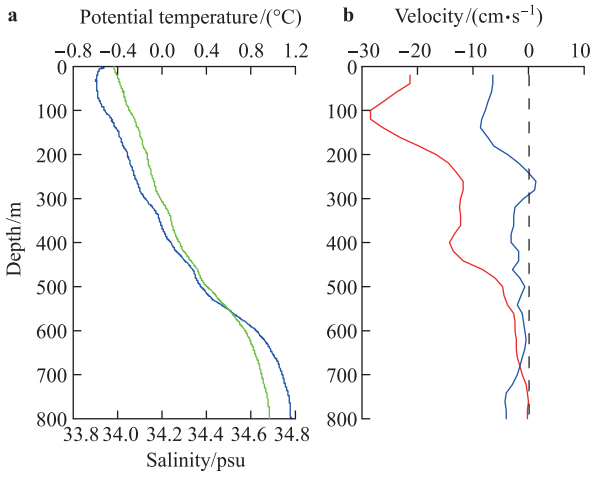

Figure 6 **a**, The mean potential temperature (blue) and salinity (green) during the yo-yo. The mean across (red) and along (blue) ice shelf front velocities. **b**, Positive values for the red line in indicate inflow and negative values outflow.

4.1 Temporal change

The yo-yo time series allowed us to examine the temporal change at the southern end of the ice shelf front. The isotherms and isohalines showed multiple vertical fluctuations during the day (Figures 3f and 3g respectively for θ and S). These isotherm fluctuations were on the order of 50 m above 500 m and 10–20 m below 500 m. Similar fluctuations of 50–100 m occurred in dissolved oxygen concentrations and meltwater content in the upper water column (Figures 3h and 3i, respectively). However, this temporal variability at the southern end (Figure 3g-3j) was weaker than the spatial variability along the front of the ice shelf (Figures 3a-3e). The currents also fluctuated temporally both in the across

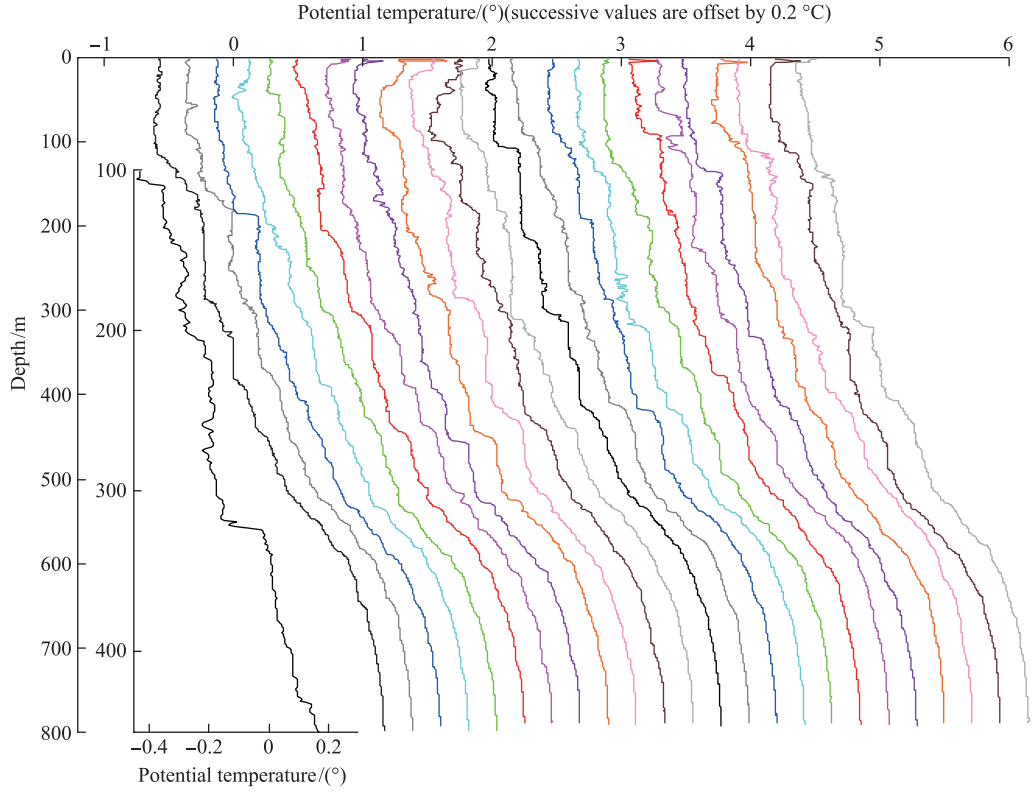

Figure 7 The 24 potential temperature profiles of the yo-yo time series, CTD casts 58–81. Profile from CTD cast16 is shown expanded on the left.

(Figure 4c) and along (Figure 4d) ice shelf front directions. Like the hydrography, velocity fluctuations were larger above 500 m than below. These temporal fluctuations are addressed more fully in the layer descriptions in section 4.5 and the temporal analysis in section 5.

4.2 Finestructure

Small scale features or finestructure appeared in θ in front of the ice shelf (Figure 3a). One measure of the size of finestructure elements is the Thorpe displacement, here the vertical distance a water parcel would move when the water column was sorted to have θ decreasing with depth from the surface[23]. Deeper than 500 m, Thorpe displacements were small, except for the deepest 200 m in the trench (CTD sites 17 and 18 in Figure 3e). Above 500 m, frequent large finestructure features exceeding 100 m occured, with these features larger in the northern section of the ice shelf front (Figure 3e). On the southern end, finestructure features were smaller, typically 25–100 m, although occasional features larger than 100 m occur. Inspection of the profiles over time (Figure 7) showed many of these features to be intrusions, although some were step-like. The finestructure at the southern end changed with time (Figure 3j) with alternating periods of increased finestructure, such as 8–13 h, and reduced finestructure, such as 5–7 h. Spatially, finestructure features were larger and more frequent higher in the water column, particularly above 300 m.

4.3 Double diffusive steps

In front of PIBIS, conditions may be suitable for the formation of double-diffusive steps. Two different types of double-diffusive steps exist: steps due to convection between two saltwater layers, with a fresher layer overlying a saltier layer and steps resulting from melting of an ice wall, although the same basic mechanism drives both. Double-diffusive convective steps between two saltwater layers occur throughout the Antarctic (e.g.[18]); however, steps resulting from melting of an ice wall, like those observed by Jacobs et al.[16] off the Erebus Glacier Tongue in McMurdo Sound, Ross Sea, are much rarer.

The structure of the water column in the southern PIBIS notch appeared to be step-like, with step sizes ranging from 5–150 m and the most common step height as 50–100 m (Figure 7). The water column to 800 m was evaluated to determine if the conditions were conducive to double-diffusive convective steps using the Turner angle, *Tu*,[24] as defined by:

$$Tu = \tan^{-1}\left(\frac{(1+R_\rho)}{(1-R_\rho)}\right). \quad (1)$$

where R_ρ is the density ratio, which was calculated from the θ and salinity gradients, $\partial\theta$ and ∂S, respectively with respect to depth, ∂z, and the thermal expansion coefficient,α, and the saline contraction coefficient, β, using

$$R_\rho = \frac{\beta \cdot \partial S/\partial z}{\alpha \cdot \partial\theta/\partial z}. \quad (2)$$

α and β were determined using the Matlab® seawater routines available on the internet (http://www.cmar.csiro.au/datacentre/ext_docs/seawater.htm). Gradients of both θ and S were determined at 1 m intervals and smoothed. The resulting *Tu* indicated the water column alternated between a stable water column (angles between –45° and 45°) and conditions conducive for weak double-diffusive convective steps (angles between –45° and 90°) (Figure 8e). The *Tu* values of roughly –30° to –45° just meet the conditions for weak steps at a few depths, primarily below 400 m. At the depths of the two most obvious large steps, 200–280 m and 330–380 m, *Tu* was stable, indicating double-diffusive steps should not exist.

In double diffusive-convective steps, there is a balance between thermal and haline effects on density. Based on this balance and laboratory experiments, Huppert and Turner[17] determined a relationship between step height, h, and the density for step generated through melting on a vertical ice wall:

$$h = 0.64\,\frac{\rho(\theta_f, S) - \rho(\theta, S)}{\partial\rho s / \partial z} \quad (3)$$

where θ_f is the θ of freezing, ρ is the density for the respective θ and S, and ρ_s is the density of water for θ_f and S at the surface. Step heights calculated using this formula and smoothed indicated theoretical step heights increasing from 10 to 25 m between 100 and 300 m depth, with the largest steps deeper in the water column (black line in Figure 8f). This disagreed with the observations of larger "steps", ~100 m higher in the water column (Figure 7). Since the ice shelf only reached to ~300 m, steps below this depth could not be from a melting ice wall, so their theoretical heights were not calculated. To estimate heights for double diffusive-convective steps, step heights, h_{Kelley}, were also calculated following Kelley's [25] formula,

$$h_{Kelley} = [0.25\times10^{-9} R_\rho^{11} \nu \kappa_T^{-1}]^{-0.25} \sqrt{\kappa_T / \langle N \rangle}\ , \quad (4)$$

as done in Robertson et al.[18], where υ is the molecular viscosity (1.85×10^{-6} m^2·s^{-1}), κ_T is the molecular diffusivity for heat (1.4×10^{-6} m^2·s^{-1}), and $\langle N \rangle$ is the vertically averaged *Brunt-Väisälä* frequency. The calculated *Kelley* step heights ranged from 1–3 m with a mean of <1 m (blue line in Figure 8f), which is less than the resolution of θ.

The observed "steps" changed rapidly in time, typically persisting less than 3 h (Figure 7). Significant changes were often seen between the down- and up-casts, roughly 0.3–0.5 h apart in time at the maximum (not shown). Padman[26] noted that distinct double-diffusive staircases are usually found where internal waves are not a major factor. Basically, the diffusivity associated with the double diffusive steps needs to exceed the mixing diffusivity. This was not the condition here, with weak stratification, N=~1–3 cph, (Figure 8c) and strong shear, 0.002–0.004 s^{-1} (Figure 8d), yielding low gradient Richardson numbers (Figure 8b). However, Padman[26] also postulated that if formed, staircases would attenuate internal waves, increasing the lifetime of the

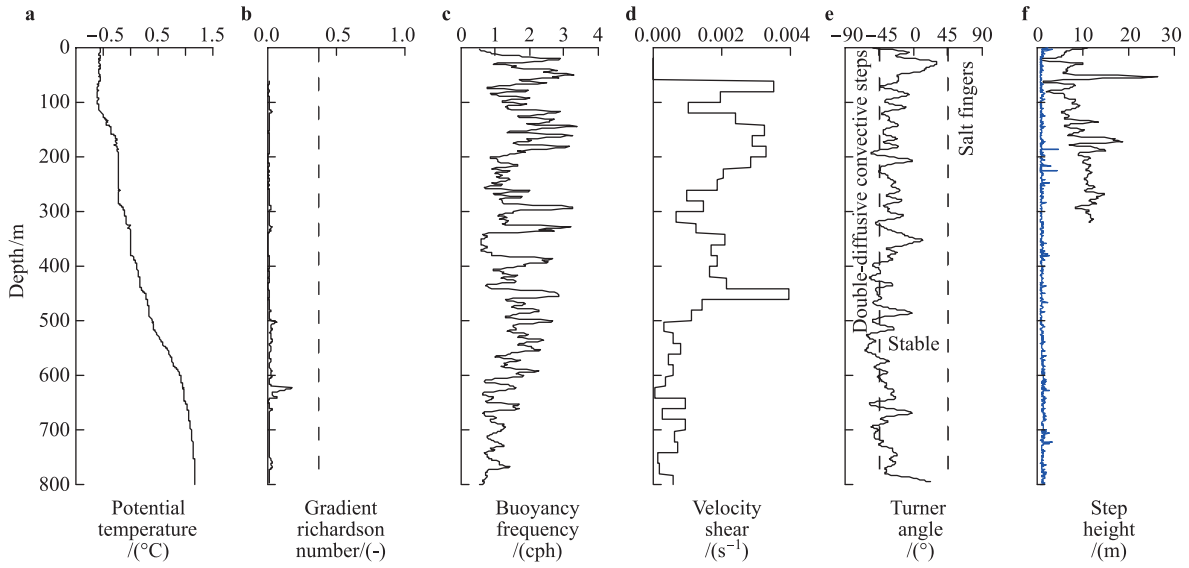

Figure 8 Profiles of potential temperature (**a**), the gradient Richardson number (**b**), the Brunt-Väisälä frequency (**c**), velocity shear (**d**), Turner Angle (**e**), and step height (**f**) for the upper 320 m, roughly the draft of the ice shelf, as for the first CTD of the yo-yo time series, cast 58. In (**f**), two calculations of step height are given, Huppert and Turner (black) and Kelley (blue). The calculated step heights following Huppert and Turner are only shown where it is applicable, in the upper 320 m, roughly the draft of the ice shelf.

steps. In their observations of steps in the Arctic near Yermak Plateau, both stratification and shear peaked at the interfaces between the observed steps. This latter scenario is more suitable for these "step" observations; however, the vertical resolution of the velocities was insufficient to resolve the interfaces and confirm this.

4.4 Intrusions

Throughout the upper 500 m of the water column, intrusions occurred frequently between water flowing out from under the ice shelf and water within PIB. These intrusions were thicker, sharper, and stronger in the upper 300 m (Figures 3 and 7). Intrusions at the southern end were less frequent, thinner, and weaker relative to those in profiles along the rest of the ice shelf front (Figure 3). These intrusions were either short lived or were advected away by the currents within an hour, before the next CTD cast. Often they disappeared between the down- and up- casts for a single CTD, less than 30 min. There was no definitive correlation between either the across or along ice shelf velocities and the occurrence of individual intrusions; however, intrusions were less frequent during stronger outflow. The intrusions appeared to be small in horizontal extent, less than 180 m, otherwise they would be observed in both the up- and down-casts with the mean currents observed here. Possible explanations for the relative scarcity, small size, and weakness of the intrusions are: (1) the water column was horizontally more uniform in θ at this location, (2) the flow was both steady and from a more uniform region, and (3) intrusions were being mixed quickly removing their signature.

4.5 Layering

At the southern notch of PIBIS, the water column behaved differently in each of several layers. At the surface, a mixed layer changed with time, primarily dependent on the wind and solar radiation (Figure 7). The well-mixed portion ranged between 10 and 80 m, typically extending to ~40 m. At various times, the upper 100 m showed sharp intrusions and evidence of solar heating. There were two primary layers: an upper layer from ~100 m to 450 m and a lower layer from 550 m to the sea bed, ~925 m (Figure 9c). Transition layers existed between the upper layer and both the surface mixed layer and the lower layer. Within the transition layers, behavior was influenced by processes of both of the adjacent layers.

4.5.1 Upper layer

The upper layer had a high meltwater content, 1%–2% and extended from 100 to 450 m. It was further divided into two sub-layers, with the division occurring at ~300 m, roughly the average draft of the ice shelf. Upper ISW layer #1 extended from 100 to 300 m and upper ISW layer #2 from 320 to 450 m, with a narrow transition region between them. As will be shown later, the behavior between these two sub-layers differed, primarily in the variability of θ and the mean velocities. A change in upper ISW layer #1 also occurred around 225 m, which was the local ice shelf depth near the southern notch.

The upper layer changed quickly with θ profiles often differing between down- and up-casts (Figure 9c). Both "steps" and intrusions occurred frequently in the upper layer. The interfaces between layers and "steps" often shifted vertically. The "steps" were present or absent in different casts and could not be tracked for more than a few hours, often changing within 20–60 min; however, the interfaces between the primary layers could be traced throughout the entire time period (Figure 7).

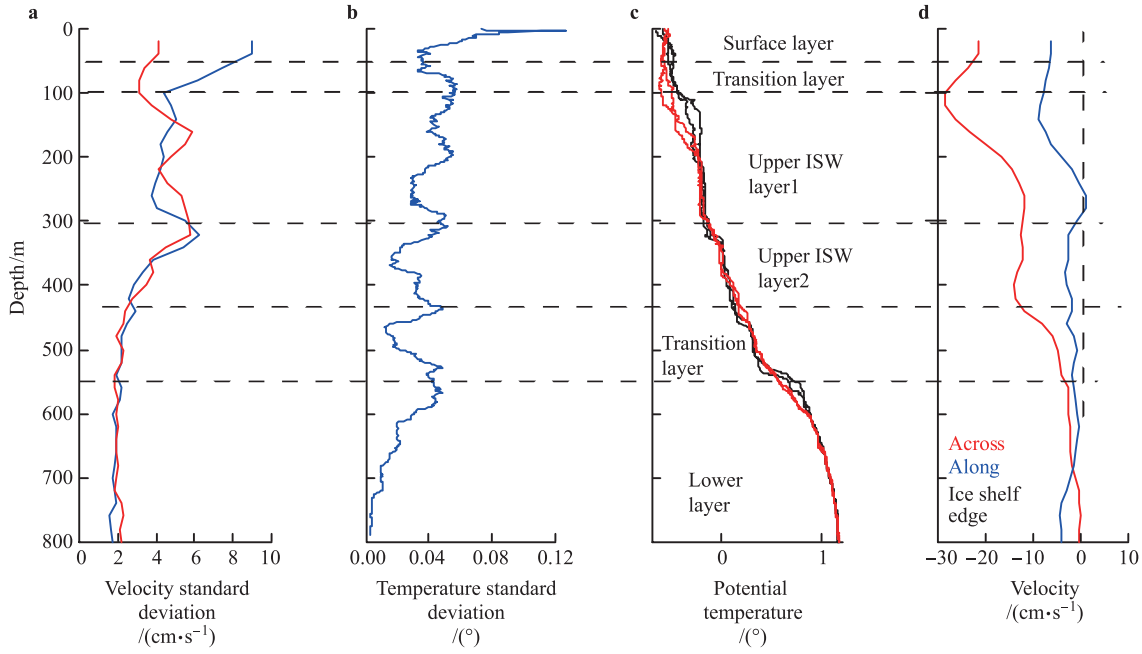

Figure 9 The standard deviation of the across (red) and along (blue) ice shelf velocities (**a**) and the temperatures (**b**) with depth. A profile of the potential temperature with depth with the layers identified for casts 16 (black) and 58 (red) (**c**). Mean across (red) and along (blue) ice shelf velocities during the yo-yo (**d**). In (**c**) the two lines represent the down and up casts.

With the exception of the surface mixed layer, depths of high θ variability coincided with the interfaces between layers, as seen in the θ standard deviations (Figure 9b). High variability at the interfaces was expected, since fluctuations of a layer of constant θ will show little variability, whereas fluctuation of an interface between layers with different θ yields high variability. Thus, the high standard deviations indicated the extents of the layers with small standard deviations in the midst of the layers. The mean U (red line in Figure 9d) decreased with depth from a peak value of 28 cm·s^{-1} to 10 cm·s^{-1} between 100 and 300 m, roughly within upper ISW layer #1 (Figure 9d). In upper ISW layer #2, U was relatively constant with depth at ~12 cm·s^{-1} (red line in Figure 9c). The currents fluctuated with time in the upper layer (100–450 m) (Figure 10), where the velocity anomaly was the difference between the velocity at each depth and mean velocity of the water column at that time. The velocity fluctuations are more fully analyzed in section 5.

4.5.2 Lower layer

The lower layer, with θ exceeding 0.6°C, was composed of mCDW (Figure 3). The flow was primarily out of the notch, U, and steady at ~2 cm·s^{-1} (Figure 4). Flow across the notch, V, ranges from 0 to a few cm·s^{-1} in or out of the notch, with the strongest flow near the bottom (Figure 4d). The resulting flow was slow, entering the cavity to the southeast. This flow was further restricted by the topography, since the notch location is in the southern part of a trench going from PIB under the ice shelf. Below 550 m, θ profiles changed very little between casts (Figure 7). Unlike the upper layer, the lower layer varied little during the observations. Comparison of profiles at this location before and after the yo-yo showed no appreciable changes in the region deeper than 550 m in the week before the yo-yo (cast 16) and a changes of ~0.06°C at depths of 550–700 m and < 0.005°C below 700 m in the 11 d after the yo-yo (cast 93). The θ change between 550–700 m appeared to be a 40 m vertical shift in the location of the thermocline.

4.6 Water column stability

Water column stability is key in determining the likelihood of mixing events such as overturns or Kelvin-Helmholtz instabilities. The gradient Richardson number, Ri_g, (Figure 8b) was determined with depth for all CTD/LADCP casts, according to

$$Ri_g = \frac{N^2}{(\partial U/\partial z)^2}. \quad (5)$$

where N is the Brunt-Väisälä frequency and $\partial U/\partial z$ the combined vertical shear in the horizontal velocities. Ri_g compares the relative stabilization of the water column by stratification as characterized by N against the destabilizing effect of the shear[27]. Gradient Richardson numbers, Ri_g, were less than 0.25, indicating an unstable water column from 50 m to the sea bed for all casts. Looking at a typical profile, CTD 58, the entire water column below the surface mixed layer was unstable according to the Ri_g (Figure 8b). Although the stratification was reasonably strong for a polar region (Figure 8c)[18,28], the strong shears in the water column (Figure 8d) overpowered the stabilizing influence of the stratification and destabilized the water column.

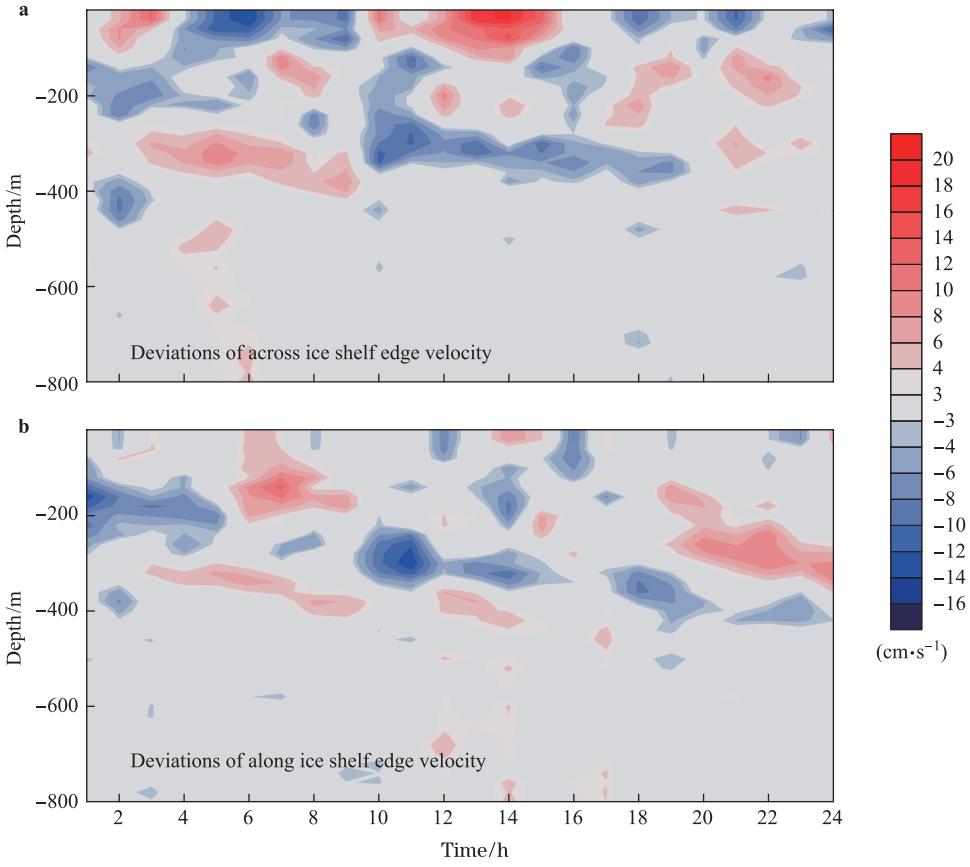

Figure 10 Anomalies in the across (**a**) and along (**b**) ice shelf front velocities in the time series.

5 Frequency distribution of the fluctuations

A variety of analysis techniques were used to identify the frequencies of the oscillations, including harmonic tidal analysis, empirical orthogonal function (EOF) analysis, spectral analysis, and a simple least squares analysis. Concerning tides, the short time series prevented separation of the M_2 and S_2 signals and identification of the individual diurnal signals, K_1 and O_1 Consequently, semidiurnal will imply the both M_2 and S_2 signals and individual constituents will not be identified in the observational data. Another factor in the semidiurnal tidal response is passage of the M_2 critical latitude through the region. The critical latitude affects the semidiurnal tidal response in several ways. First, it prevents propagation of baroclinic M_2 tides poleward of its latitude (74° 24' S), basically the ice shelf cavity. Second, resonant effects can be induced by the M_2 tide, inciting inertial oscillations. Near critical latitudes, it is essentially impossible to separate inertial oscillations from the semidiurnal tidal signal without a multi-decadal time series. Consequently, the semidiurnal signal includes inertial oscillations. It should be noted that vorticity from a wind-driven gyre present in PIB (Figure 5) effectively shifted the critical latitude 1° poleward, enabling baroclinic M_2 tides to propagate at the yo-yo site[15].

5.1 Velocities

The semidiurnal tides/inertial oscillations, as determined through tidal analysis using Pawlowicz et al.'s T_Tide software[29], varied with depth (Figure 11a) from ~11cm·s^{-1} near the surface to 1 cm·s^{-1} near the bottom. Since only a 24 h time series was available for this analysis, uncertainties were quite high. The tidal currents in the lower mCDW layer were weak, with major axes of 1–2 cm·s^{-1} and relatively uniform with depth (Figure 11a). Both the minor axes and inclination of the tidal ellipses were relatively uniform within this layer (Figures 11c and 11e, respectively). In the upper layer, the major axes of the tidal ellipses varied with depth from 7 cm·s^{-1} to 1 cm·s^{-1}. Although there was a general decreasing trend in the major axes, bands of high semidiurnal tidal activity occurred around 150 and 300 m and low tidal activity at 100, 230, and 300 m. The bands of high tidal activity occurred in regions of θ gradients, not within the layers (Figures 11a and 11g). The bands of low tidal activity coincided with areas which are vertically well-mixed, i.e. layers. Baroclinic tides propagate well though a stratified medium, but not through a homogenous medium, although they will propagate horizontally between layers. The bands of low tidal activity resulted from vertically propagating internal semidiurnal tides encountering a more homogeneous region, where their propagation changed due to the different, lower Brunt-Väisälä frequency, N. The minor axes of the tidal ellipses were also small, <2 cm·s^{-1} within the upper layer (Figure 11c). The inclinations of the tidal ellipses showed three different basic values within the

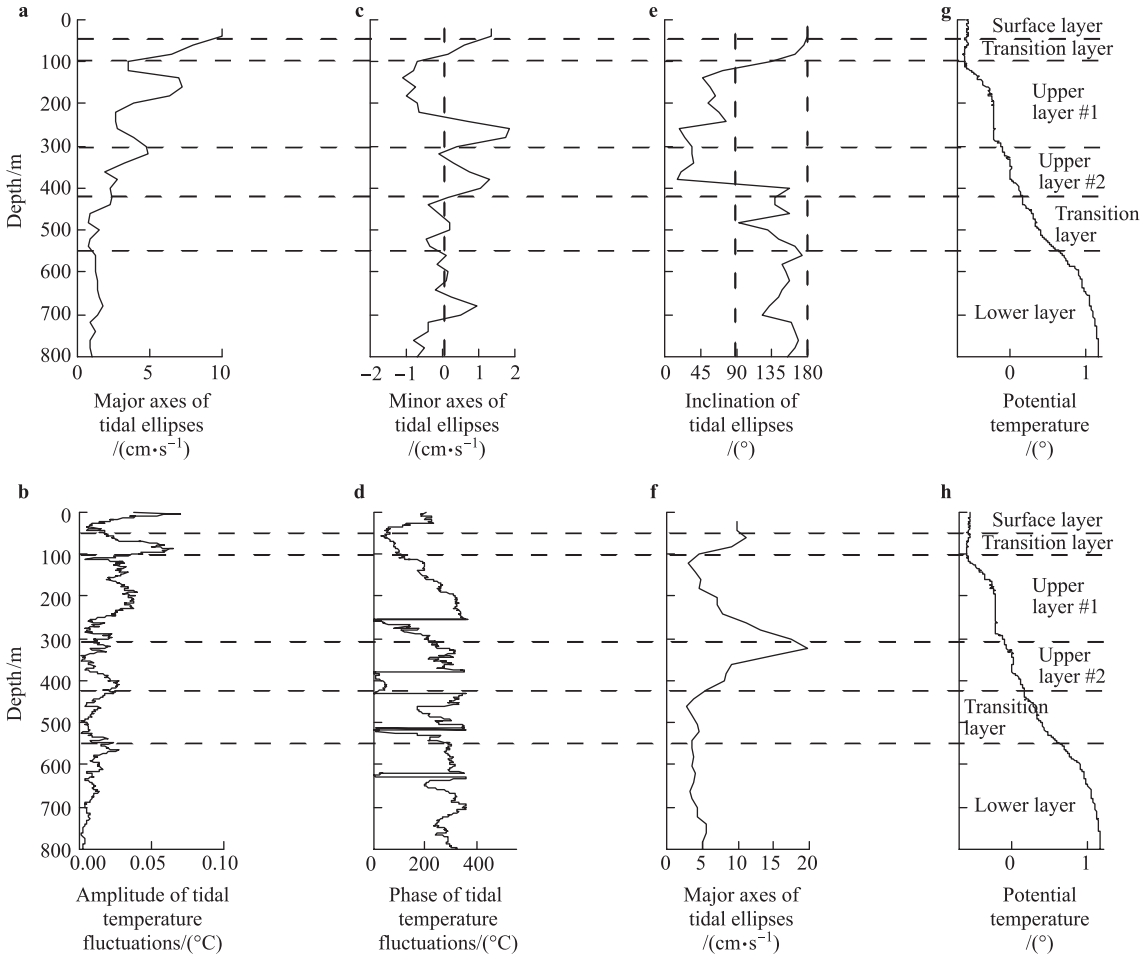

Figure 11 The major axes (**a**), minor axes (**c**), and inclinations (**e**) of the semidiurnal tidal ellipses as determined in the velocity data. A profile of the potential temperature (**g**) with the layers indicated is shown for reference. The amplitude (**b**) and phases (**d**) of the semidiurnal tidal ellipses as determined in the potential temperature data. The major axes of the tidal ellipses as determined through least squares analysis for diurnal constituents (**f**). A profile of the potential temperature with the layers indicated is again shown for reference (**h**).

upper layer (Figure 11e), coinciding with the three θ gradient sections (Figure 11g). In the uppermost of these sections, the inclination was ~60°, in the middle section ~30° and in the lower section ~140°. The ice shelf at this location extended to ~220 m and appeared to have influenced the upper section. Generally, the PIBIS depth extends to ~300 m, which is within the middle section. The lower gradient is well below the depth of the ice shelf and should not be steered by the ice shelf. The upper two sections appear affected by the ice shelf and the nearby iceberg.

Further evidence for vertical propagating waves was given by the EOF analysis. In the upper layer, a definite two peak signal occurred between 100 and 400 m. This signal was stronger in the along ice shelf direction, with 21.1% of the variability, than in the across ice shelf direction, 7.2% (not shown). The time signature of the second EOF was roughly semidiurnal. Semidiurnal energy in the along ice shelf direction had vertical wavelengths of ~75, 150, and 450 m (not shown). The first of these agreed with the width of the uppermost EOF fluctuation (not shown), the second with the band of two peaks in the EOF fluctuation, and the third roughly with the thickness of the primary layers. The across ice shelf velocities had vertical wavelengths ranging from approximately 400 m, roughly the two primary layer thicknesses, to 50 m (not shown). More energy occurred in vertical wavelengths greater than 100 m, indicating generally the water column moves in the two layers. But the wide range of vertical wavenumbers at this frequency indicated energy transfers from the long wavelengths to shorter wavelengths through nonlinear interactions.

The distribution of the spectral density with depth and frequency supports the layered response of the water column (Figure 12) At the semidiurnal frequency (2 cpd), spectral densities were roughly one order of magnitude higher in the upper layer versus the lower layer in both the along and across ice shelf velocities (Figure 12). Higher spectral levels also occurred from 3–10 cpd in the upper layer, particularly in upper ISW layer #1. The highest spectral energy was present in the surface layer at frequencies from 1–3 cpd for the across ice shelf velocities, which was the direction of the wind during this time. Spectral densities in the lower layer were much lower, primarily around the semidiurnal frequency (Figure 12).

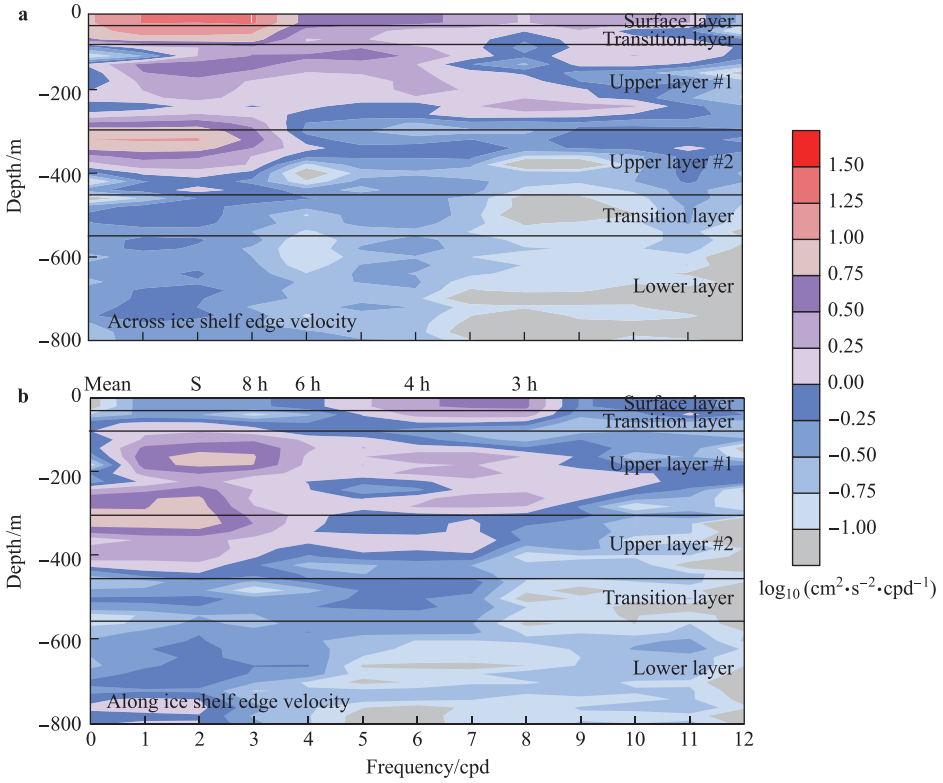

Figure 12 The log of the spectra of the across (**a**) and along (**b**) ice shelf front velocities with depth. Layer extents are labeled as are the prominent periods with S indicating semidiurnal.

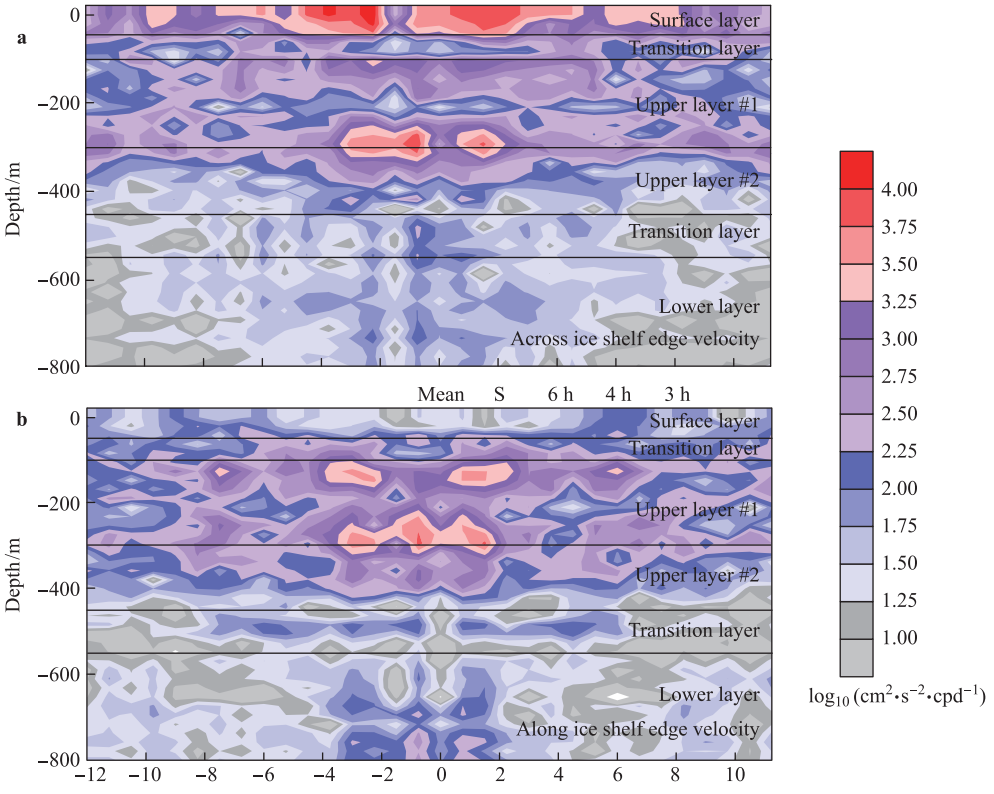

Figure 13 The log of the bispectra of the across (**a**) and along (**b**) ice shelf front velocities for the semidiurnal frequency with depth. Layer extents are labeled as are the prominent frequencies with S indicating semidiurnal.

The transfer of energy from the semidiurnal frequency to other frequencies and the layered response were supported by bispectra for the semidiurnal frequency with depth (Figure 13). In the lower layer, there was much less energy transfer than in the upper layer and most of the energy was transferred from the 2 cpd frequency to the 1 cpd frequency and the harmonics for both velocities. In the upper layer, energy was transferred from the 2 cpd frequency to a wide range of high frequencies and the 1 cpd frequency (Figure 13). The largest energy transfers in the across ice shelf front velocities occurred in the surface layer and at the interface between the two upper layers, roughly the average depth of the ice shelf. For the along ice shelf front velocities, the peak energy transfers occurred again at the interface between the two upper layers and just below the upper limit of upper ISW layer #1. These peak energy transfers coincided with the peak values in both the semidiurnal major axes (Figure 11a) and the EOF analysis (not shown). The energy transfer from the semidiurnal to the 1 cpd frequency also coincided with the peak at 300 m in the harmonic analysis (Figure 11f).

5.2 Potential temperatures

Although typically velocities are better suited for frequency analysis, the higher vertical resolution and lower uncertainties for θ enabled a more comprehensive picture in the θ signals. A strong signal at the semidiurnal/inertial oscillation frequency was apparent in θ (Figures 11b and 11f) with a much finer vertical resolution. It is unusual to observe such strong signals in temperature compared to velocity, since tidal signals in temperature are generally not as robust as those for velocities and temperature signals rely on a gradient being present. There was a general decrease in the amplitude of the tidal θ fluctuations with increasing depth throughout the water column, but like the velocities, bands of high and low activity occurred at the semidiurnal frequency, with amplitude peaks generally coinciding with layer boundaries, as expected. Amplitudes were higher in the upper layer. In the lower layer, semidiurnal θ fluctuations are small, ~0.01–0.025°C (Figure 11b), yet still exceeded the instrument accuracy. Again, the uncertainties were large due to the short time series; however, the θ signal is more definitive than that of the velocities. The phase in the lower layer was generally uniform at ~330° (Figure 11d), indicating the lower layer is moving in unison. The behavior was different in the upper layer. Like the velocities, θ showed a banding pattern with higher values generally coinciding with gradients and lower values coinciding with mixed portions (Figure 11b). The phase changed gradually, increasing with depth (Figure 11d) and indicated a propagating internal tide with the phase propagating down and the energy up. Note that the phase "wrapped" around at about 250 m, despite the axes extending beyond 360°. The phase change was more

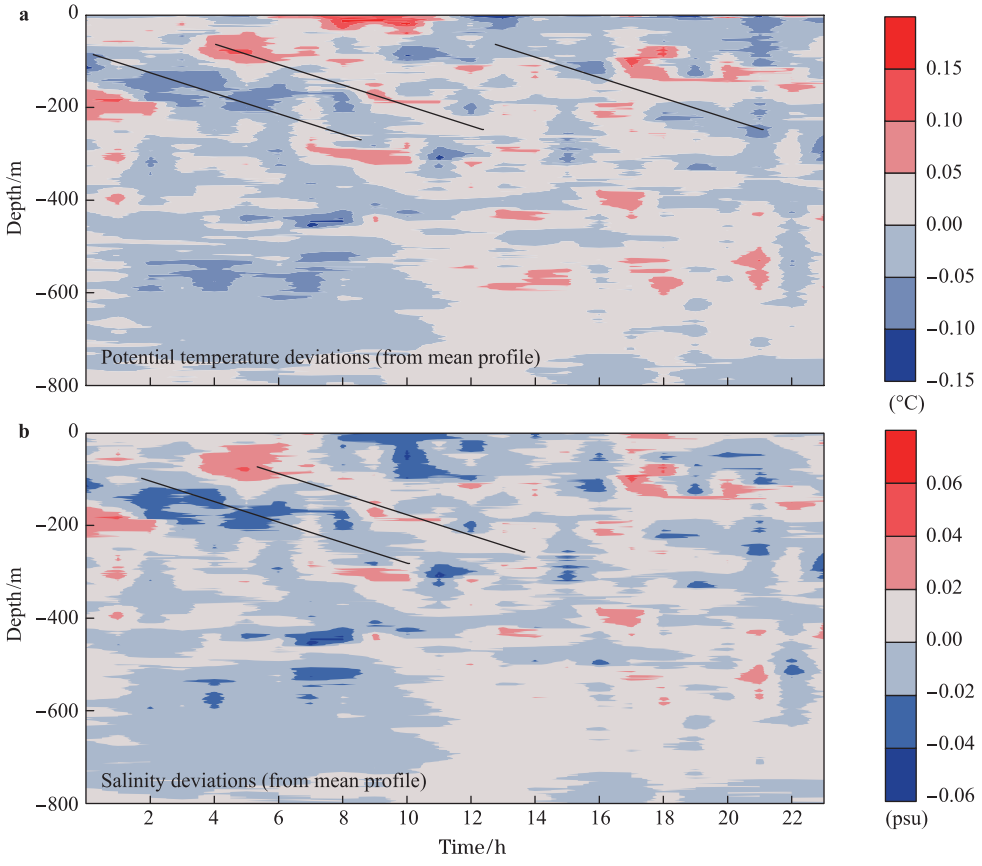

Figure 14 Potential temperature (**a**) and salinity anomalies (**b**) in the time series of CTD data with the downward propagation of the anomalies indicated by lines.

evident between 100–300 m in the region above the depth of the ice shelf than between 300–450 m and less apparent in the mixed portions.

Vertical propagation was evident in θ and S anomalies with time (Figure 14). The θ anomalies were defined as the difference between θ at a depth and the temporal mean of θ for that depth. Salinity anomalies were defined likewise. The propagation of cold and warm anomalies between 100 and 300 m were clear in the θ anomalies (Figure 14a). Cold anomalies occurred twice during the period, indicating a semidiurnal tide or an inertial oscillation. The θ anomalies were accompanied by corresponding salinity anomalies, indicating some density compensation (Figure 14b).

Spectra of the temperature with depth indicated a strong response at the semidiurnal and 24 h frequencies (Figure 15) in both θ and S. The spectral density was highest in the upper layer (Figure 15). At the interfaces between layers and in the middle of upper ISW layer #1, high spectral density occurred at a wide band of frequencies, 2–10 cpd. However, cross-spectra between the across and along ice shelf front velocities with θ indicated that it fluctuated with the velocities primarily at a low frequency, ~1 cpd, (not shown). Thus, the primary fluctuations were probably attributable to the diurnal tide. There was some evidence that θ also fluctuates with the across ice shelf front velocities at higher harmonics, again with the highest spectral density at the interfaces between layers and the middle of upper ISW layer #1 (not shown).

6 Discussion

The general structure of the water column in the outflowing southern end of the PIB ice shelf front was ISW over mCDW with a steppy-structure and finestructure in the upper 500 m. Although the Turner angle (Figure 9e) indicated an alternating stable water column with occasional conditions for weak double diffusive steps, the largest observed "steps" occured in the stable portions. Theoretical step heights were much smaller than the observed steps. Calculated step heights indicated there should be small steps in the upper water column and larger steps deeper (Figure 8e), which is the opposite of what was observed (Figure 7) and does not agree with the finestructure as represented by the Thorpe displacements (Figure 3j). According to Padman[26], double diffusive steps generally occur in regions where internal tidal energy is low. The observed steps changed quite rapidly, within 20–60 min and the currents at this location were quite strong (Figure 4c and 4d) with strong shear throughout the water column (Figure 8d). These indicated that this outflow region changed rapidly, in less than an hour.

Although, these "steps" could be double diffusive convective steps, an alternative explanation is that they are formed by various mixing events occurring either within the ice shelf cavity creating layers of uniform water at various depths, which flow out of the cavity. Candidates for these mixing events are (1) buoyant ISW flowing out of the ice

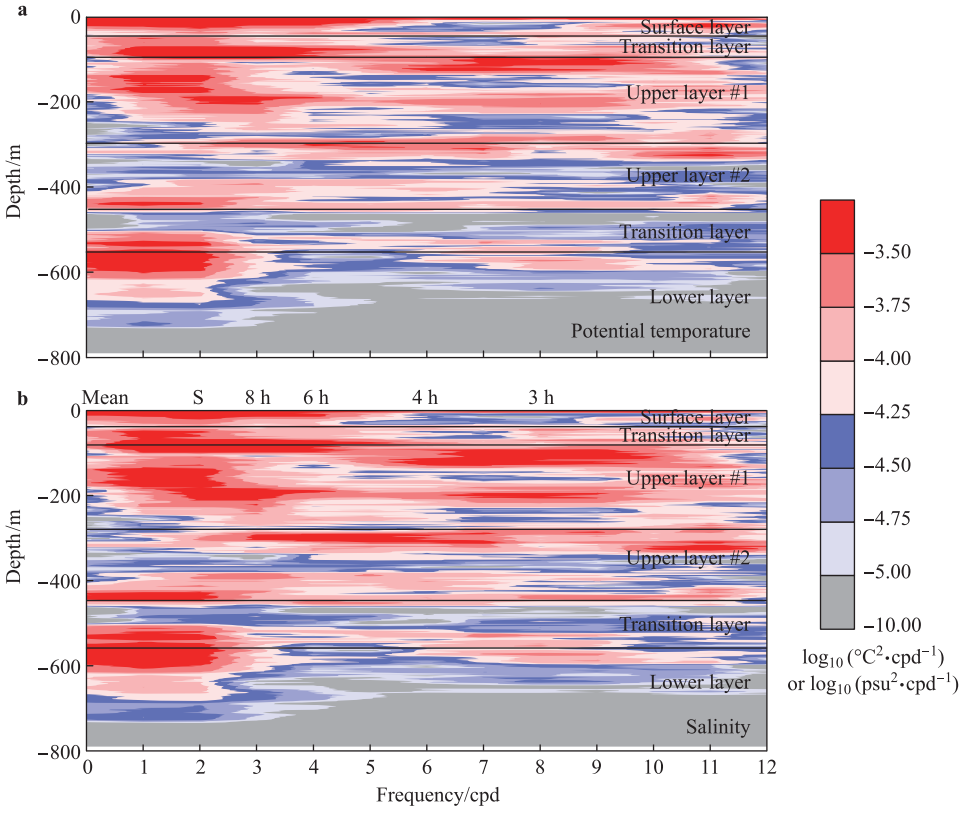

Figure 15 The log of the spectra of the potential temperature (**a**) and salinity (**b**) with depth. Layer extents are labeled as are the prominent periods with S indicating semidiurnal.

shelf cavity and mixing with the surrounding water as it flows up towards the surface and (2) internal tides and/or waves resulting from the barotropic tide interacting with the ice shelf topography or bottom topography under the ice shelf. In support of the first of these candidates, the ISW flow out of the cavity was very turbulent and boils were commonly seen in this region. Although wind is a typical mixing mechanism, wind does not act within the ice shelf cavity and within the notch in the ice shelf where the CTD data was collected, the wind and waves were fetch limited and would be insufficient to reach the depths of high variability, 100–300 m. Generation of homogenous parcels of water by breaking of internal waves through the generation of Kelvin-Helmholtz instabilities is well known and typically accepted to occur when the gradient Richardson number is less than 0.25. These conditions are met (Figure 8b). Furthermore, the most well defined steps occurred when the flow was the strongest, as shown in CTD cast 16, which was collected during a period of spring tides and the strongest observed outflow (Figure 4a).

Considering the temporal variability of θ, S, and the currents, the prime candidates for influencing the flow were wind and tides. As to tides, the yo-yo data was collected during a neap tide and reflects weaker flow and less clearly defined layers than were present during the spring tide (CTD 16). The length of the time series was insufficient to definitively identify diurnal tides, although there were indications of a 1 cpd signal. Semidiurnal tides were baroclinic and complex, with the response different in the two layers (Figure 11). In the lower mCDW layer, a weak semidiurnal tide aligned along the ice shelf existed and the tide was basically uniform for the layer. The upper ISW layer was more complex. Generally, the semidiurnal tides in the upper layer were stronger and aligned across the ice shelf front. The unique location of the yo-yo in the notch and being surrounded by the ice shelf on three sides, along with the iceberg, may have resulted in the tides being steered into the ice shelf. The semidiurnal tides in upper ISW layer #1, which extends to the depth of the base of the ice shelf, appeared to result from a combination of factors. First, the semidiurnal tides were reflected by the ice shelf. These reflections interacted nonlinearly, particularly in certain depth bands, and transferred energy to other frequencies, including the diurnal and higher frequency internal waves, as evidenced by spectra (Figure 12) and bispectra (Figure 13). Bands of high frequency energy coincided with the limits of this upper ISW layer #1 and the peak for 1 cpd at 300 m (Figure 11f). There was evidence of internal tides propagating downward in this layer. Linear internal wave theory predicts no propagation of the M_2 semidiurnal tide (absence of blue line in Figure 16a) and a downward propagation of the S_2 semidiurnal tide (red line in Figure 16a). Just north of the critical latitude, propagation of M_2 internal tides is relatively horizontal (blue lines in Figure 16b). Since the ice shelf front is poleward of the M_2 critical latitude, 78°28' S, theoretically any internal waves formed there should not propagate, but be trapped and dissipate. However, the relative vorticity of the gyre in PIB is sufficient to shift the

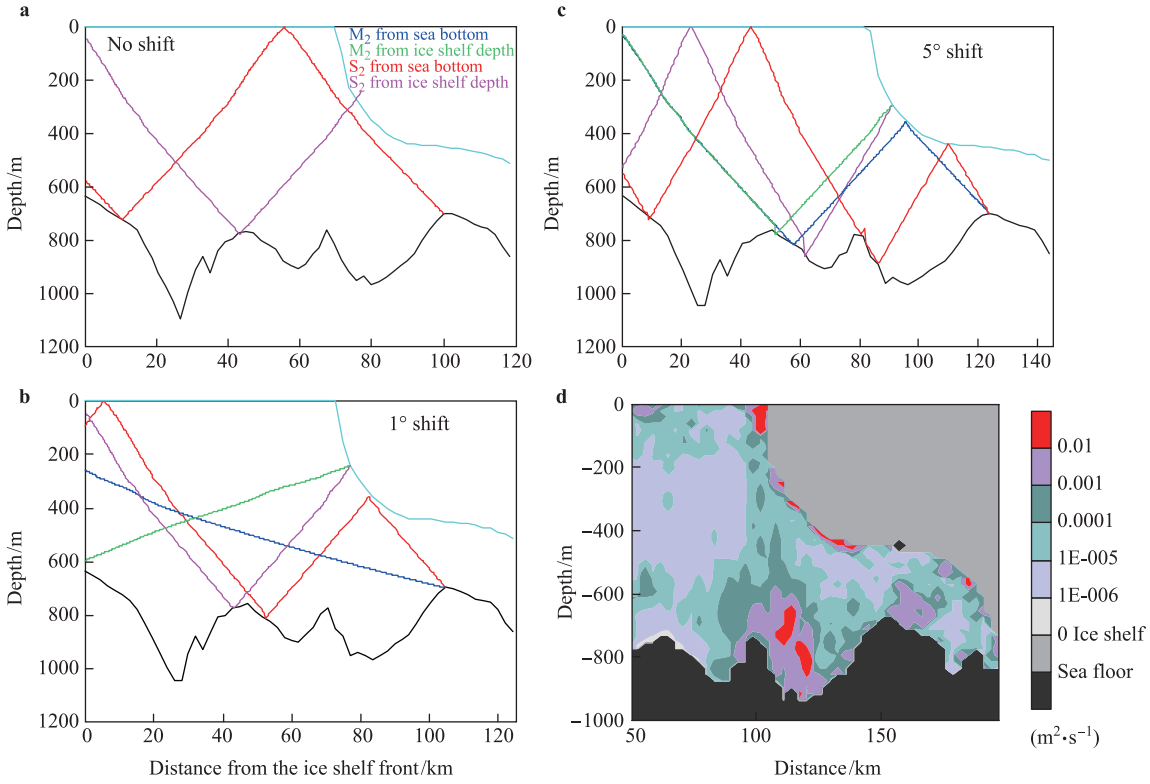

Figure 16 The slope of the theoretical internal wave rays for the semidiurnal tides (**a**) with M_2 in blue and K_1 in red at the true location and shifted poleward by 1° (**b**) and 5° (**c**). The sea bed is indicated by the black line and the ice shelf by a cyan line. Diffusivities of temperature in Pine Island Bay and under the ice shelf from a simulation with a wind-driven gyre (data from Robertson[15]) (**d**).

critical latitude 1°–5° poleward, increasing M_2 baroclinic tide generation and enabling the M_2 tide to propagate, as shown in Figures 16b and 16c, respectively, for the M_2 (blue lines) and S_2 (red lines) internal wave beams generated at the ice shelf front or base[15]. The 1° shift reflects the conditions observed during the observational period and the 5° shift a potential shift which could occur with a stronger wind-driven gyre. Note that the M_2 (blue lines) propagate nearly horizontal for the 1° shift, but with the 5° shift, they propagate down through the entire water column.

The horizontal wavelength for the internal semidiurnal tides propagating downward is ~46 km, roughly the size of PIB. The θ anomalies propagate at 0.006 cm·s^{-1}, which is roughly equivalent to the theoretical propagation speed of a semidiurnal tide for this stratification and location, 0.005 cm·s^{-1}. A resonant, semidiurnal internal tide propagating in this basin in upper ISW layer #1 matches this behavior. In upper ISW layer #2, which is below the base of the ice shelf, the semidiurnal tides are weaker, shift direction, and are aligned with the ice shelf. Potential temperature changes in this layer were not well correlated with changes in velocity, indicative of multiple water sources. Finally, although no definitive identification of the semidiurnal tidal constituent was possible, the semidiurnal response was more likely to be S_2 than M_2, since TPXO8.0[20] and a regional model indicate S_2 is stronger here[15].

The transfer of energy from the semidiurnal tides to higher wavenumber tides and/or higher frequency waves has important implications for mixing. These interactions could easily contribute to mixing in this region. The small mixing events observed in this data are consistent with tidal mixing. The M_2 internal wave propagation is nearly horizontal. This sets up the conditions for inducing Kelvin-Helmholtz instabilities at the interfaces, resulting in the formation of other small mixed patches. These mixed patches would have uniform properties, which would appear step-like. A simulation of tides for this region showed high temperature diffusivities at the ice shelf front both along the bottom of the ice shelf and over the sea bed (Figure 16d)[15]. The model includes mixing due to shear instabilities from the internal tides, but not mixing due to interactions of tides and/or waves reflected from the ice shelf. There are also high diffusivities over the ridge, indicating potential mixing there. Although inertial oscillations and semidiurnal tidal frequencies are quite close at this location, inertial oscillations do not propagate. The signals here at the semidiurnal tidal frequency propagated and were more likely to be due to internal semidiurnal tides than inertial oscillations. Tides appeared to induce mixing in front of the ice shelf and may be responsible for mixing under the ice shelf. Additionally, along with tides, the buoyant flow out from under the ice shelf is naturally a dominant factor in mixing the outflowing ISW and meltwater.

7 Summary

CTD and LADCP data from a survey in PIB and a 24 h time series in the southern notch of the PIBIS were examined to determine the water column structure and its temporal variability and the role of double-diffusion and tides in this variability. Inspection of a transect across the front of the ice shelf indicated that the southern notch was probably in a strong outflow region, since it had the highest percentage of meltwater along the front of the ice shelf, the strongest outflowing currents, and the warmest, saltiest water with the lowest dissolved oxygen concentration in the upper water column.

The water column in this region consisted of a 10–80 m thick surface mixed layer and two major layers: the upper and lower layers (Figure 17). The upper layer ranged from 100 to 450 m, showed a mean flow exiting the ice shelf cavity, and had a high meltwater signal, ~2%. The upper layer was further split into 2 layers, upper ISW layer #1 and upper ISW layer #2. Upper ISW layer #1 extended roughly from 100–300 m, had the highest meltwater percentage, and was strongly influenced by the ice shelf, with its base at ~300 m. Upper ISW layer #2 extended from 320–450 m, had a lower meltwater percentage, and showed less ice shelf influence. The lower layer was composed of mCDW, ranged from 550 m to the sea bed, and its mean flow was into the ice shelf cavity. Between the two major layers and between the two sub-layers in the upper layer were transition layers, which were affected by processes of both of the adjacent layers. The lower layer was relatively stable during this time period and showed little variability. In contrast, the upper layer was very active, changed rapidly, and had frequent intrusions. Throughout the water column step-like features were present and changed rapidly. These features were more pronounced, larger, and changed within an hour in the upper layers. However, theoretical double diffusive step heights did not agree with the observed step height, although the conditions for weak double diffusive convective steps were occasionally met below the depth of the base of the ice shelf. These step-like features may be double diffusive steps or alternatively, the results of various mixing events within or upon exit of the ice shelf cavity. Two potential candidates for these mixing events are inverse sill flow as the ISW exits the cavity and internal tides and waves. Double diffusive steps from an ice wall such as observed by Jacobs[16] off the Erebus Glacier Tongue were not observed in this location.

A majority of the temporal fluctuations were attributable to tides or their harmonics. Thurnherr et al.[9] also noted temporal variability at this location was consistent with low frequency internal gravity waves. Superimposed on a barotropic signal with roughly a 24 h period were two diurnal peaks in amplitude exceeding 10 cm·s^{-1}. One of these peaks was at the surface and coincided with a peak in the semidiurnal amplitude. The other peak was centered at approximately the depth of the keel of the ice shelf. Both of these peaks are believed to be semidiurnal tides or their harmonics, which resulted from nonlinear interactions of the tides with the ice shelf topography. The semidiurnal tides were complex. Basically the semidiurnal tides were baroclinic with a weak tide aligned along the ice shelf front in the lower

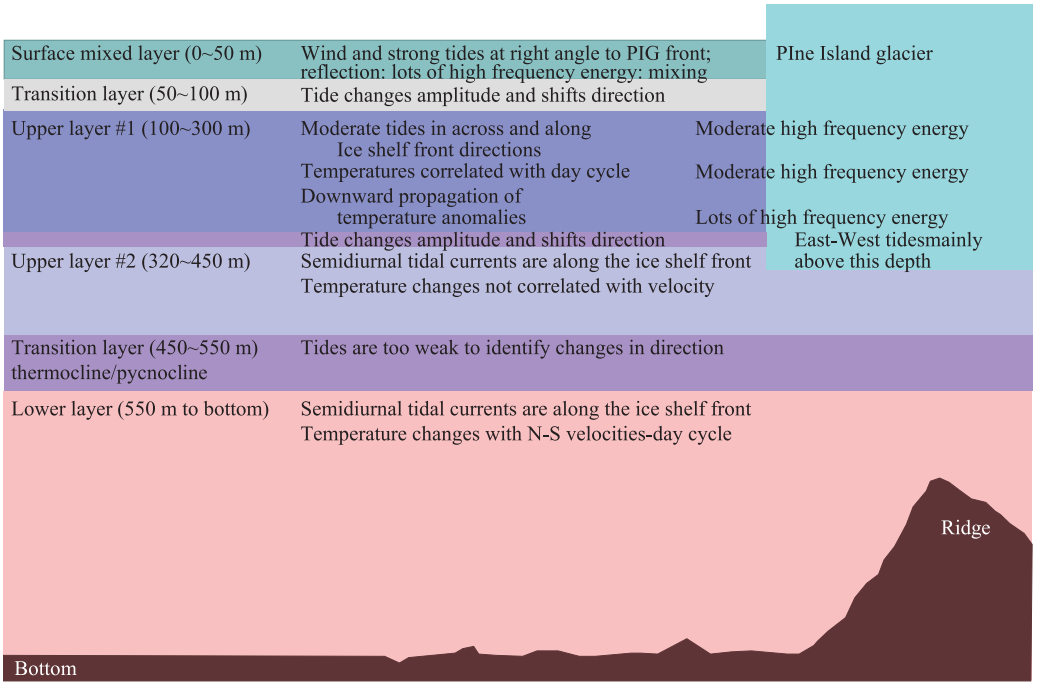

Figure 17 Overview of the tidal response in the different layers of the water column.

mCDW layer (550 m to the bottom), ~1 cm·s^{-1}, and stronger tides aligned across the ice shelf front in upper ISW layer #1 (100 m to 450 m). The strongest tides occurred in the upper 20 m and reached 10 cm·s^{-1}. In upper ISW layer #1, mode 2 baroclinic semidiurnal tides were found be propagating between 100 and 300 m, both in the velocities and in the θ and salinity anomalies. This depth range coincided with the upper of the two ISW layers. The propagation rate of these tides agreed with the propagation rate of mode 2 semidiurnal tides with a horizontal wavelength of ~46 km, which was roughly equivalent to the diameter of PIB, opening a strong possibility of resonant phenomena playing a role. The semidiurnal tide showed a wide range of vertical wavelengths during this time period indicating transfer of energy through nonlinear interactions from the long wavelength barotropic tide into shorter wavelength, higher mode waves with the same frequency. Energy was also found at higher frequencies than the tidal frequencies, particularly 3 and 4 h periods. Bispectra indicated energy transfers from the semidiurnal tides to a period of ~24 h, possibly the diurnal tides, and to higher harmonic frequencies. Furthermore, these energy transfers occurred in distinct depth bands, corresponding to the surface and the limits of upper ISW layer #1. Since the semidiurnal tide in this region was directed into the ice shelf, these energy transfers were likely due to interactions of the semidiurnal tide with its reflection off the ice shelf front below 100 m. This is also the region of the resonant propagating waves.

This is in no way a definitive treatment of the structure of the water column off the PIG and its temporal variability. The 24 h time series is too short, less than the diurnal cycles and only resolves two semidiurnal cycles. It represents only the conditions on that day. However, until data from a mooring with instruments in the upper water column is placed either in this region or on the ice shelf for a longer time period, this is the best picture we have of the processes in this location. Such a mooring is unlikely to survive a long term deployment, due to iceberg activity in the region and the relatively rapid movement of the ice shelf, making it unlikely a long time series of data will be collected any time soon. Any data collected for this region increases the knowledge base of this critical region and contributes to our understanding of the processes taking place. Future work to understand the ocean driving forces causing the melting and determining the outflow will encompass both obtaining more observational data both in front of and under the ice shelf and using models to fill in the gaps in the observational data and isolate the role of the different processes.

Acknowledgements I would like to thank the crew and support personnel on the RVIB *Nathaniel B. Palmer* during NPB0901, Stan Jacobs for providing me the opportunity of participating in the research voyage, and the people who collected the CTD data: Katherine Leonard, Christopher Little, and Kenneth Mankoff. Thanks are also due to Pierre Dutrieux for providing the shipboard ADCP data and first noting the gyre in PIB. Additionally, I would like to thank the anonymous reviewers who made valuable suggestions resulting in significant changes to this paper. This project was funded partially by both the Australian Antarctic Division, project 2944.

References

1 Rignot E, Bamber J L, van den Broeke M R, et al. Recent Antarctic ice mass loss from radar interferometry and regional climate modeling. Nat Geosci, 2008, 1(2): 106–110

2 Payne A J, Viela A, Shepherd A P, et al. Recent dramatic thinning of

largest West Antarctic ice stream triggered by oceans. Geophys Res Lett, 2004, 31(23): L23401, doi: 10.1029/2004GL021284
3 Shepherd A, Wingham D, Rignot E. Warm ocean is eroding West Antarctic Ice Sheet. Geophys Res Lett, 2004, 31(23): L23402, doi: 10.1029/2004GL021106
4 Pritchard H D, Ligtenberg S R M, Fricker H A, et al. Antarctic Ice Sheet loss driven by basal melting of ice shelves. Nature, 2012, 484(7395): 502–505, doi: 10.1038/nature10968
5 Christianson K, Bushuk M, Dutrieux P, et al. Sensitivity of pine island glacier to observed ocean forcing. Geophys Res Lett, 2016, 43(20): 10817–10825, doi: 10.1002/2016GL070500
6 Jenkins A, Dutrieux P, Jacobs S S, et al. Observations beneath Pine Island Glacier in West Antarctica and implications for its retreat. Nat Geosci, 2010, 3(7): 468–472
7 Jenkins A. Convection-driven melting near the grounding lines of ice shelves and tidewater glaciers. J Phys Oceanogr, 2011, 41(12): 2279–2294, doi: 10.1175/JPO-D-11-03.1
8 Jacobs S S, Jenkins A, Giulivi C F, et al. Stronger ocean circulation and increased melting under Pine Island Glacier ice shelf. Nat Geosci, 2011, 4(8): 519–523
9 Thurnherr A M, Jacobs S S, Dutrieux P, et al. Export and circulation of ice cavity water in Pine Island Bay, West Antarctica. J Geophys Res, 2014, 119(3): 1754–1764, doi: 10.1002/2013JC009307
10 Dutrieux P, Vaughan D G, Corr H F J, et al. Pine Island glacier ice shelf melt distributed at kilometre scales. Cryosphere, 2013, 7(5): 1543–1555
11 Dutrieux P, De Rydt J, Jenkins A, et al. Strong sensitivity of Pine Island ice-shelf melting to climatic variability. Science, 2014, 343(6167): 174–178
12 Robertson R. Tidally induced increases in melting of Amundsen sea ice shelves. J Geophys Res, 2013, 118(6): 3138–3145, doi: 10.1002/jgrc.20236
13 Jacobs S S, Huppert H E, Holdsworth G, et al. Thermohaline steps induced by melting of the Erebus Glacier tongue. J Geophys Res, 1981, 86(C7): 6547–6555
14 Huppert H E, Turner J S. On melting icebergs. Nature, 1978, 271(5640): 46–48
15 Robertson R, Padman L, Levine M D. Fine structure, microstructure, and vertical mixing processes in the upper ocean in the western Weddell Sea. J Geophys Res, 1995, 100(C9): 18517–18535
16 Jacobs S, Jenkins A, Mankoff K, et al. Cruise report for NBP09-01. https://www.bodc.ac.uk/data/information_and_inventories/cruise_inventory/report/nathanielbpalmer0901.pdf, 2009
17 Garrett C. Internal tides and ocean mixing. Science, 2003, 301(5641): 1858–1859
18 Egbert G D, Erofeeva S Y. Efficient inverse modeling of barotropic ocean tides. J Atmos Oceanic Technol, 2002, 19(2): 183–204
19 Jacobs S, Jenkins A, Hellmer H, et al. The Amundsen Sea and the Antarctic Ice Sheet. Oceanography, 2012, 25(3): 154–163
20 Jenkins A, Jacobs S. Circulation and melting beneath George VI Ice Shelf, Antarctica. J Geophys Res, 2008, 113(C4): C04013, doi: 10.1029/2007JC004449
21 Thorpe S A. Turbulence and mixing in a Scottish Loch. Phil Trans Roy Soc A, 1977, 286(1334): 125–181, doi: 10.1098/rsta.1977.0112
22 Schmitt R W. Double diffusion in oceanography. Ann Rev Fluid Mech, 1994, 26(1): 255–285
23 Ruddick B. A practical indicator of the stability of the water column to double-diffusive activity. Deep Sea Res A, 1983, 30(10): 1105–1107
24 Padman L. Momentum fluxes through sheared oceanic thermohaline steps. J Geophys Res, 1994, 99(11): 22491–22499
25 Turner J S. Buoyancy effects in fluids. Cambridge: Cambridge University Press, 1973: 368
26 Robertson R, Visbeck M, Gordon A L, et al. Long-term temperature trends in the deep waters of the Weddell Sea. Deep Sea Res II, 2002, 49(21): 4791–4806
27 Pawlowicz R, Beardsley R, Lentz S. Classical tidal harmonic analysis including error estimates in MATLAB using T_TIDE. Comp Geosci, 2002, 28(8): 929–937
28 Timmermann R, Le Brocq A, Deen T, et al. A consistent data set of Antarctic Ice Sheet topography, cavity geometry, and global bathymetry. Earth Syst Sci Data, 2010, 2(2): 261–273, doi: 10.5194/essd-2-261-2010
29 Nitsche F O, Jacobs S S, Larter R D, et al. Bathymetry of the Amundsen sea continental shelf: implications for geology, oceanography, and glaciology. Geochem Geophys Geosyst, 2007, 8(10): Q10009, doi: 10.1029/2007GC001694